Iran University of Science and Technology

International Journal of

Railway Research

ISSN: 2423-3838

Vibration Analysis of a Hybrid Levitation Pod with Compressor Unbalanced Force in Hyperloop System

Hamed Petoft [1], Vahid Fakhari [2], Abbas Rahi *[3]

[1] Ph.D. Candidate, Faculty of Mechanical and Energy Engineering, Shahid Beheshti University, Tehran, Iran
[2] Assistant Professor, Faculty of Mechanical and Energy Engineering, Shahid Beheshti University, Tehran, Iran
[3*] Assistant Professor, Faculty of Mechanical and Energy Engineering, Shahid Beheshti University, Tehran, Iran

ARTICLE INFO

Article history:
Received: 19.10.2022
Accepted: 18.04.2023
Published: 30.04.2023

Keywords:
Hyperloop
EMS
Air cushions
Unbalancing parameter
Frequency
Resonance

A B S T R A C T

Hyperloop Transportation Technology (HTT) is a worldwide invention proposed by Elon Musk in the last decade. This system works based on moving an ultra-high-speed capsule-shaped vehicle called a "pod" into low-air pressure tubes. In this paper, we conceptually designed a large-sized industrial pod equipped with an axial compressor. Also, we considered an unbalanced centrifugal force on the compressor blades. The novel-designed pod has two suspensions simultaneously, including magnetic levitation (EMS kind) and air cushion technology. We applied the air cushions to overcome the overall weight of the pod. Also, we used magnets for the motion stability of the pod. The present study proposes a 5-DOF dynamic model for the system containing the pod's vertical and lateral displacements and the body pitching, rolling, and yawing angles. In this regard, the natural frequencies are verified using simulating the system in ADAMS software. Afterward, we analytically calculated the natural frequencies and system responses by applying the impedance matrix method. In the numerical results, we analyzed the pod responses, when the resonance phenomenon occurs for undamped and damping cases. Results showed oscillations increased by increasing the unbalancing parameter. We finally investigated the effect of two main design parameters containing the pod's total mass and stiffness of the air cushions on the natural frequencies. Increasing the air cushion's stiffness and decreasing the total mass generally increase the natural frequencies.

1. Introduction

Hyperloop is an ultra-high-speed cargo or passenger transportation system. This system was fisrt introduced by Elon Musk at the end of the year 2013 [1]. This system works based on moving a very high-speed capsule-shaped vehicle called the "pod" into the low-air pressure tubes. There are two different separate technologies for levitating the pod. The first is magnetic levitation, and the second is air cushion suspension. The systems with air cushions are equipped with an axial compressor in front of the pod. Magnetic levitation itself is divided into three different types. They are Electro-Magnetic Suspension (EMS), Electro-Dynamic Suspension (EDS), and Inductrack systems. EMS vehicles work based on the attraction force between the vehicle and guideway magnets. Vice versa, in EDS systems, the train is levitated by the repulsive force of the vehicle and guideway magnets[2]. Inductrack is a passive, fail-safe EDS system, using only unpowered

*Corresponding author
Email address: a_rahi@sbu.ac.ir

loops of wire in the guideway and the body magnets with Halbach arrays [3].

Some researchers tried to present an appropriate dynamic model for the hyperloop system, high-speed maglev trains, and air cushion vehicles.

Pradhan and Katyayan [4] experimentally designed a small-sized pod called “Orcapod” for the Hyperloop world competitions. Then, they proposed a four Degree-Of-Freedom (DOF) dynamic model for the pod. Their model was a half-vehicle model with two pairs of flexible EDS (inductrack) permanent magnets at the front and rear of the pod. They obtained the system's natural frequencies and determined the pod vibrational mode shapes. Madhan et al. [5] designed a small-sized wheeled pod equipped with six angular magnetic modules. Then, they analyzed the pod vibrations as a 9-DOF model containing the vertical displacements of the body and modules, as well as the body pitching and rolling angles. They used Simulink MATLAB software and Newmark numerical method to solve the model. They also investigated the effects of acceleration and braking on the system's vibrational behavior.

Paval et al. [6] simulated the airflow inside the air cushion cavity of a hovercraft system with an elliptic shape using Ansys Fluent software. In their model, the air gap between the cushion and the ground and air velocity were the input parameters. They calculated the cushion lift force, static pressure, and mass flow rate in different gaps and air velocities. They also designed and investigated other models for air cushions with different shapes and suspensions[7-9].

Wu et al. [10] analyzed the coupling vibrations of the vehicle guideway for a high-speed train. They investigated the effect of inner loop current gain coefficient, time lag, and levitation current perturbation on the static stability of the vertical suspensions for the maglev vehicle using the full-vehicle model with five EMS frames. The model included the vertical displacement, pitching, and rolling angles for the body and frames (without lateral displacement or guidance forces effects). They used the double loop control principle to suppress the vehicle and guideway vibrations. Wang et al. [11] presented fuzzy Proportional–Integral–Derivative (PID) control for reducing the dynamic oscillations of a high-speed maglev train-bridge interaction. They used a half-vehicle model with four EMS frames interacting with a bridge as the simply-supported beam model.

Using an air compressor for the hyperloop system has many advantages, including air suction and helping to reduce the drag force of the air inside the tube to the pod, providing the compressed air needed by the air cushions, providing the oxygen required for passengers through the air storage tanks, and also helping to propel the pod forward. But the presence of an air compressor in front of the pod can be a factor in destabilizing the pod's movement. We describe this issue in detail in the paper.

As it is clear, in the design of mechanical systems, it is never possible to accurately make the components of the designed parts symmetrical and balanced in terms of mass distribution in all segments of the part production. There is always a small percentage of error due to mass imbalance. Especially in the case of mechanical rotating systems, this phenomenon becomes more visible and effective. Therefore, this phenomenon is not far from expected in the case of the air compressor, which consists of air suction turbine blades.

A group of researchers investigated dealing with this issue with various compressors and vehicles with different approaches. They also described how this phenomenon affects the system’s performance. Seve et al. [12-14] investigated the balancing of a variable-speed rotary compressor with experimental and numerical methods. They used the Finite Element (FE) model, based on the rotor dynamics theory in connection with the Influence Coefficient Method (ICM). They compared numerical and experimental unbalance responses obtained with different balancing criteria. The proposed balancing method satisfies both the vibration level minimization criterion and its industrial implementation. Ferraris et al. [15] studied the influence of cylinder pressure on the balancing of a rotary compressor. They expanded the cylinder pressure force into a Fourier series, evaluating the bearing characteristics, establishing the balancing, and predicting the compressor response. They used rotor dynamics, FE, and ICM to reduce the vibration levels of the rotor and stator parts of the compressor.

Wang et al. [16] investigated the effect of dynamic unbalance of the underframe suspended

rotational equipment on the flexible vibrations of the car body of a high-speed train. They showed that underframe dynamic unbalance can affect car body vibrations, especially the local flexible vibration, which causes decrease in the passenger ride comfort and may even cause structural damage to the car body. They showed that decreasing the unbalanced mass of the rotational equipment can reduce car body vibrations. In addition, utilizing the elastic suspension as a Dynamic Vibration Absorber (DVA) for the underframe equipment can isolate the vibration transmission to the car body. Jitendra Kumar [17] designed a linear DVA for an unbalanced blower rotor (caused by a broken blade). He used the blower with the two-Degree-Of-Freedom (2-DOF) model and studied two different strategies for the location of DVA. The results showed the positive effect of DVA on vibration response reduction of the blower. Zhang et al. [18] presented a numerical model to analyze the dynamic behaviors of the crankshafts in single-cylinder and twin-cylinder rotary compressors. They assumed the crankshaft centrifugal force as the unbalanced force generated by the crank part and roller. They used upper and lower balancers on the motor rotor to reduce this centrifugal force.

Aziaka et al. [19] conceptually designed an axial compressor for a large industrial gas turbine. They mentioned that unbalancing is the main factor of vibrations in axial compressors and may damage bearings and seals in part of their research. Even in some conditions, it causes component failure or fatigue. Unbalancing occurs when the center of the mass is not located at the rotating center. They proposed balancing the system by putting the shaft on the knife edge.

As mentioned earlier, the existence of an air compressor in front of the pod, despite its advantages, can be a factor in destabilizing the pod's movement. This problem results in an unbalanced force caused by the non-uniform distribution of mass in the asymmetric part applying as a disturbing external excitation force to the system. If the excitation frequency of this external force is equal to the natural frequency of the system, for the undamped system case, the resonance phenomenon occurs and causes instability. We investigated this issue in the present research in detail. Therefore, we first present a 5-DOF model for the pod. The proposed pod is equipped with both air cushions and EMS magnets simultaneously. We simulated the system in ADAMS software and verified the introduced model by comparing the natural frequencies obtained. Then, we studied the unbalanced force's effect on the vibration and instability of the pod using analytical and numerical methods. Also, we investigate the influence of the unbalancing parameter and damping of the air cushions on the vibration behavior of the pod for its related movements. Finally, we analyze the effect of two pod design parameters containing the total mass of the pod and stiffness of air cushions on the natural frequencies.

2. Proposed Pod Modeling

In this section, we present the proposed pod model briefly and usefully. This innovative conceptual model includes both air cushions and EMS levitations simultaneously. We used air cushions to overcome the overall weight, and EMS magnets are responsible for motion stability and accelerating the pod. Therefore, it is necessary to calculate the number of air cushions required to overcome the pod weight and suspend the system. But, first, we present the proposed pod dynamic model and derive governing equations. Then, we will describe our air cushions modeling and the related calculations in the next section concisely.

2.1. Five DOF Pod Model

In this section, the conceptual pod model is presented as follows:

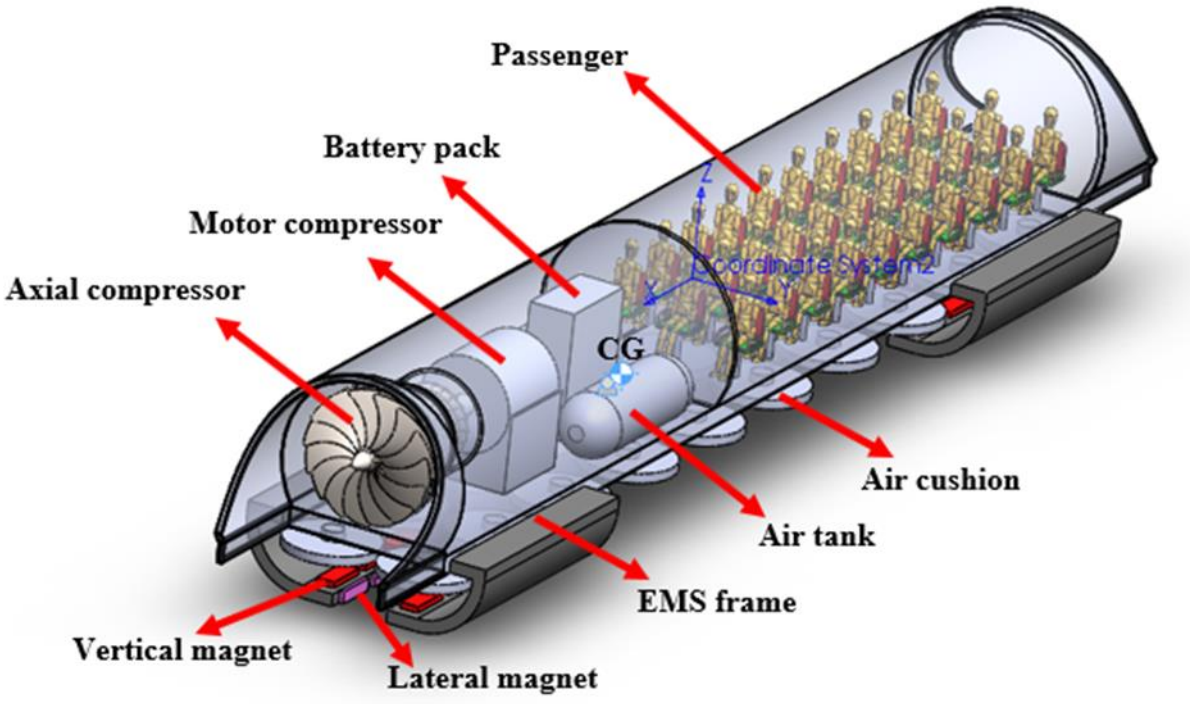

Fig. 1: Proposed pod model with its components

The system's technical specifications is provided in the Appendix section. The main dimensions of the pod are taken from Elon Musk's report [1]. However, the dynamical properties of the pod are calculated using the "mass properties evaluation" command in SolidWorks. These parameters are the total weight of the pod, three mass moments of inertia, and the Center of Gravity (CG). All moments of inertia are considered relative to the CG position of the pod. The technical specifications of the EMS part are reported according to Min et al. [20] numerical data.

Two pairs of frames are located at the front and rear of the pod that support the vertical and lateral magnets. As mentioned earlier, the air cushions are responsible for overcoming the overall weight, and EMS magnets are used for motion stability and accelerating the pod. Also, we utilized the lateral magnets for the pod lateral motion stability. In this regard, we derived the governing dynamic equations as follows:

$$\sum F_Z = m\ddot{z}$$

$$m\ddot{z} + \sum_{i=1}^{10} K_{ar_i}(z \mp L_i\theta + W\varphi) + \sum_{i=1}^{10} K_{al_i}(z \mp L_i\theta - W\varphi) + \sum_{i=1}^{10} C_{ar_i}(\dot{z} \mp L_i\dot{\theta} + W\dot{\varphi}) + \sum_{i=1}^{10} C_{al_i}(\dot{z} \mp L_i\dot{\theta} - W\dot{\varphi})$$
$$+K_{z1}(z - L_f\theta + a\varphi) + K_{z2}(z - L_f\theta - a\varphi) + K_{z3}(z + L_r\theta + a\varphi) + K_{z4}(z + L_r\theta - a\varphi) - \sum_{j=1}^{4} K_{Ij}\, I_j = 0 \quad (1)$$

$$\sum F_y = m\ddot{y}$$

$$m\ddot{y} + \sum_{j=1}^{2} K_{yj}(y \pm h\varphi + L_f\psi) + \sum_{j=3}^{4} K_{yj}(y \pm h\varphi - L_r\psi) + \sum_{j=1}^{4} K_{Iyj}\, I_{yj} = 0$$

$$\sum M_G = I_{yy}\ddot{\theta}$$

$$I_{yy}\ddot{\theta} \pm \sum_{i=1}^{10} K_{ar_i} L_i (z \mp L_i\theta + W\varphi) \pm \sum_{i=1}^{10} K_{al_i} L_i (z \mp L_i\theta - W\varphi) \pm \sum_{i=1}^{10} C_{ar_i} L_i \left(\dot{z} \mp L_i\dot{\theta} + W\dot{\varphi}\right)$$
$$\pm \sum_{i=1}^{10} C_{al_i} L_i \left(\dot{z} \mp L_i\dot{\theta} - W\dot{\varphi}\right) - K_{z1} L_f \left(z - L_f\theta + a\varphi\right) - K_{z2} L_f \left(z - L_f\theta - a\varphi\right)$$
$$+ K_{z3} L_r (z + L_r\theta + a\varphi) + K_{z4} L_r (z + L_r\theta - a\varphi) + \sum_{j=1}^{2} K_{Ij}\, I_j L_f - \sum_{j=3}^{4} K_{Ij}\, I_j L_r = 0$$

$$\sum M_G = I_{xx}\ddot{\varphi}$$

$$I_{xx}\ddot{\varphi} + \sum_{i=1}^{10} K_{ar_i} W (z \mp L_i\theta + W\varphi) - \sum_{i=1}^{10} K_{al_i} W (z \mp L_i\theta - W\varphi) + \sum_{i=1}^{10} C_{ar_i} W \left(\dot{z} \mp L_i\dot{\theta} + W\dot{\varphi}\right) -$$
$$\sum_{i=1}^{10} C_{al_i} W \left(\dot{z} \mp L_i\dot{\theta} - W\dot{\varphi}\right) + K_{z1} a \left(z - L_f\theta + a\varphi\right) - K_{z2} a \left(z - L_f\theta - a\varphi\right) + K_{z3} a (z + L_r\theta + a\varphi) -$$
$$K_{z4} a (z + L_r\theta - a\varphi) \pm \sum_{j=1}^{2} K_{yj} \left(y \pm h\varphi + L_f\psi\right) h \pm \sum_{j=1}^{2} K_{yj} (y \pm h\varphi - L_r\psi)\, h \pm \sum_{j=1}^{4} K_{Ij}\, I_j\, a \pm \sum_{j=1}^{4} K_{Iyj}\, I_{yj}\, h = 0$$

$$\sum M_G = I_{zz}\ddot{\psi}$$

$$I_{zz}\ddot{\psi} + \sum_{j=1}^{2} K_{Iyj}\, I_{yj} L_f + \sum_{j=3}^{4} K_{Iyj}\, I_{yj} L_r + \sum_{j=1}^{2} K_{yj} \left(y \pm h\varphi + L_f\psi\right) L_f - \sum_{j=3}^{4} K_{yj} (y \pm h\varphi - L_r\psi) L_r = 0$$

where z and y are the vertical and lateral displacements, θ, φ, and ψ are the pitching, rolling, and yawing angles respectively. For other parameters, m is the pod total mass, K_{ar_i} is the i^{th} stiffness of the air cushion on the right side of the pod, K_{al_i} is the i^{th} stiffness of the air cushion on the left side of the pod, and similarly, C_{ar_i}, is the damping coefficient of the i^{th} air cushion on the right side, C_{al_i}, is the damping coefficient of the i^{th} air cushion on the right side of the pod, L_i is the longitudinal distance between the i^{th} air cushion and the center of mass (CG), $L_f = \frac{L}{2} - X_M - X_{CG}$ is the longitudinal distance between front magnets and CG, $L_r = \frac{L}{2} - X_M + X_{CG}$ is the longitudinal distance between rear magnets and CG, K_{z1}, K_{z2}, K_{z3}, and K_{z4}, respectively are the front left, front right, rear left, and rear right vertical magnet stiffness. The same argument is also valid for the lateral magnets. W is the lateral distance between air cushions and CG, a is the lateral distance between the magnets and CG, and h is the vertical distance between the magnets and CG. It should be noted that I_j and I_{yj} are the j^{th} vertical and lateral magnetic current intensities, K_{Ij} and K_{Iyj} are the j^{th} vertical and lateral magnetic current coefficients.

By sorting each relation of Eq. 1 according to the variables and also by assuming equality of stiffness and damping coefficients for all cushions with K_a and C_a, the equations are simplified as follows:

$$m\ddot{z} + (20K_a + K_1)z + (20C_a)\dot{z} + \left(2K_a\bar{L} + L_rK_2 - L_fK_3\right)\theta + (2C_a\bar{L})\dot{\theta} + (K_4 + K_5)a\varphi - K_{I1}I_1 - K_{I2}I_2 - K_{I3}I_3 - K_{I4}I_4 = 0$$

$$m\ddot{y} + K_{1y}y + \left(K_{4y} + K_{5y}\right)h\varphi + \left(K_{3y}L_f - K_{2y}L_r\right)\psi + K_{Iy1}\,I_{y1} - K_{Iy2}\,I_{y2} + K_{Iy3}\,I_{y3} - K_{Iy4}\,I_{y4} = 0$$

$$I_{yy}\ddot{\theta} + \left(2K_a\bar{L} + L_rK2 - L_fK_3\right)z + (2C_a\bar{L})\dot{z} + \left(2K_a\bar{L}^2 + {L_r}^2K_2 + {L_f}^2K_3\right)\theta + (2C_a\bar{L}^2)\dot{\theta} + \left(L_rK_4 - L_fK_5\right)a\varphi + K_{I1}L_fI_1 + K_{I2}L_fI_2 - K_{I3}L_rI_3 - K_{I4}L_rI_4 = 0 \quad (2)$$

$$I_{xx}\ddot{\varphi} + (K_4 + K_5)az + \left(K_{1y}\right)hy + \left(L_rK_4 - L_fK_5\right)a\theta + \left(20K_aW^2 + K_1a^2 + \left(K_{4y} + K_{5y}\right)h^2\right)\varphi + (20C_aW^2)\dot{\varphi} + \left(K_{4y}L_r - K_{5y}L_f\right)h\psi + K_{I1}I_1a - K_{I2}I_2a + K_{I3}I_3a - K_{I4}I_4a + K_{Iy1}I_{y1}h - K_{Iy2}I_{y2}h + K_{Iy3}I_{y3}h - K_{Iy4}I_{y4}h = 0$$

$$I_{zz}\ddot{\psi} + \left(K_{3y}L_f - K_{2y}L_r\right)y + \left(K_{4y}L_r - K_{5y}L_f\right)h\varphi + \left(K_{3y}{L_f}^2 + K_{2y}{L_r}^2\right)\psi + K_{Iy1}\,L_fI_{y1} - K_{Iy2}\,L_fI_{y2} - K_{Iy3}\,L_rI_{y3} + K_{Iy4}\,L_rI_{y4} = 0$$

In the simplified Eq. 2, $\bar{L} = 27.1$ ($\bar{L} = L_1 \pm L_2 \pm \cdots \pm L_{10}$) is the sum of the longitudinal distances between the air cushions on each side and the CG, which is the negative sign for the front of CG and is positive for the rear of CG. Also, $\bar{L}^2 = 403.441\ m^2$ ($\bar{L}^2 = {L_1}^2 + {L_2}^2 + \cdots + {L_{10}}^2$) is the sum of the squared distances between the air cushions on each side and CG, and other coefficients are defined as follows:

$$\begin{gathered} K_1 = K_{z1} + K_{z2} + K_{z3} + K_{z4} \\ K_2 = K_{z3} + K_{z4} \\ K_3 = K_{z1} + K_{z2} \\ K_4 = K_{z4} - K_{z3} \\ K_5 = K_{z2} - K_{z1} \\ \\ K_{1y} = K_{y1} + K_{y2} + K_{y3} + K_{y4} \\ K_{2y} = K_{y4} + K_{y3} \\ K_{3y} = K_{y2} + K_{y1} \\ K_{4y} = K_{y4} - K_{y3} \\ K_{5y} = K_{y2} - K_{y1} \end{gathered} \quad (3)$$

Now, we use the EMS formula to calculate the equivalent stiffness coefficients caused by air cushions and the stiffness and current coefficient of vertical and lateral magnets. Therefore, first, the main relationship for calculating the vertical and lateral forces of an EMS-type system is expressed as follows:

$$\begin{gathered} F_z(i_z, z) = \frac{\mu_0 A_m N^2 {i_z}^2}{4z^2} \\ F_y\left(i_y, y\right) = \frac{\mu_0 A_m N^2 {i_y}^2}{4y^2} \end{gathered} \quad (4)$$

In Eq. 4, F_z and F_y are the vertical and lateral (known as guidance force) EMS forces which are a function of parameters containing the vertical i_z, z, and lateral i_y, y, current and gap. Also, the constant coefficients of this relationship include $\mu_0 = 4\pi \times 10^{-7}\,\frac{H}{m}$ magnetic permeability coefficient in the vacuum, $A_m = 0.1\ m^2$ cross-sectional area of magnets, and $N = 330$ number of coil turns. As seen in Eq. 4, the EMS formula for calculating the vertical (levitation) and lateral (guidance) forces are similar. The only difference is that one is defined in the vertical and the another in the lateral direction. In Eq. 4, by linearizing the EMS levitation and guidance forces formula about the stable vertical $i_{0z} = 15\ A$, $z_0 = 10\ mm$, and lateral $i_{0y} = 20\ A$, $y_0 = 10\ mm$ current and gap, we have:

$$\Delta F_z = \left|\frac{\partial F_z}{\partial i_z}\right|_{(i_{0z},z_0)} i_z(t) + \left|\frac{\partial F_z}{\partial z}\right|_{(i_{0z},z_0)} z(t) = K_{Ij} i(t) + K_{zj} z(t)$$

$$K_{Ij} = \frac{\mu_0 A_m N^2 i_{0zj}}{2{z_0}^2}, \quad K_{zj} = -\frac{\mu_0 A_m N^2 {i_{0zj}}^2}{2{z_0}^3}$$

$$\Delta F_y = \left|\frac{\partial F_y}{\partial i_y}\right|_{(i_{0y},y_0)} i_y(t) + \left|\frac{\partial F_y}{\partial y}\right|_{(i_{0y},y_0)} y(t) = K_{Iyj} i(t) + K_{yj} y(t) \quad (5)$$

$$K_{Iyj} = \frac{\mu_0 A_m N^2 i_{0yj}}{2{y_0}^2}, \quad K_{yj} = -\frac{\mu_0 A_m N^2 {i_{0yj}}^2}{2{y_0}^3}$$

After defining and explaining these parameters, we calculate the mass, stiffness, and damping coefficients of the presented equations of Eq. 2. The governing equations can be described in the matrix form as $M\ddot{X} + C\dot{X} + KX = F$, where $X = [z \quad y \quad \theta_{yy} \quad \varphi_{xx} \quad \psi_{zz}]^T$ is the matrix of variables and F is the matrix external forces.

Considering that the system is assumed to be in a steady state with a constant current intensity in both directions ($i_y = i_{y0}$, $i_z = i_{z0}$) and there isn't any disturbing external force, so $F = 0$. Thus, the remaining coefficients of the matrix can also be obtained as follows:

$$M = \begin{bmatrix} m & 0 & 0 & 0 & 0 \\ 0 & m & 0 & 0 & 0 \\ 0 & 0 & I_{yy} & 0 & 0 \\ 0 & 0 & 0 & I_{xx} & 0 \\ 0 & 0 & 0 & 0 & I_{zz} \end{bmatrix}$$

$$K = \begin{bmatrix} 20K_a + K_1 & 0 & 2K_a\bar{L} + L_rK_2 - L_fK_3 & (K_4 + K_5)a & 0 \\ 0 & K_{1y} & 0 & (K_{4y} + K_{5y})h & K_{3y}L_f - K_{2y}L_r \\ 2K_a\bar{L} + L_rK_2 - L_fK_3 & 0 & 2K_a\bar{L}^2 + {L_r}^2K_2 + {L_f}^2K_3 & (L_rK_4 - L_fK_5)a & 0 \\ (K_4 + K_5)a & (K_{4y} + K_{5y})h & (L_rK_4 - L_fK_5)a & 20K_aW^2 + K_1a^2 + (K_{4y} + K_{5y})h^2 & (K_{4y}L_r - K_{5y}L_f)h \\ 0 & K_{3y}L_f - K_{2y}L_r & 0 & (K_{4y}L_r - K_{5y}L_f)h & K_{3y}{L_f}^2 + K_{2y}{L_r}^2 \end{bmatrix} \quad (6)$$

$$C = \begin{bmatrix} 20C_a & 0 & 2C_a\bar{L} & 0 & 0 \\ 0 & 0 & 0 & 0 & 0 \\ 2C_a\bar{L} & 0 & 2C_a\bar{L}^2 & 0 & 0 \\ 0 & 0 & 0 & 20C_aW^2 & 0 \\ 0 & 0 & 0 & 0 & 0 \end{bmatrix}$$

2.2. Air Cushions Modeling and Performed Calculations

In this section, the dynamic modeling of the air cushions is presented. In this regard, we first introduce the air cushions modeling as follows:

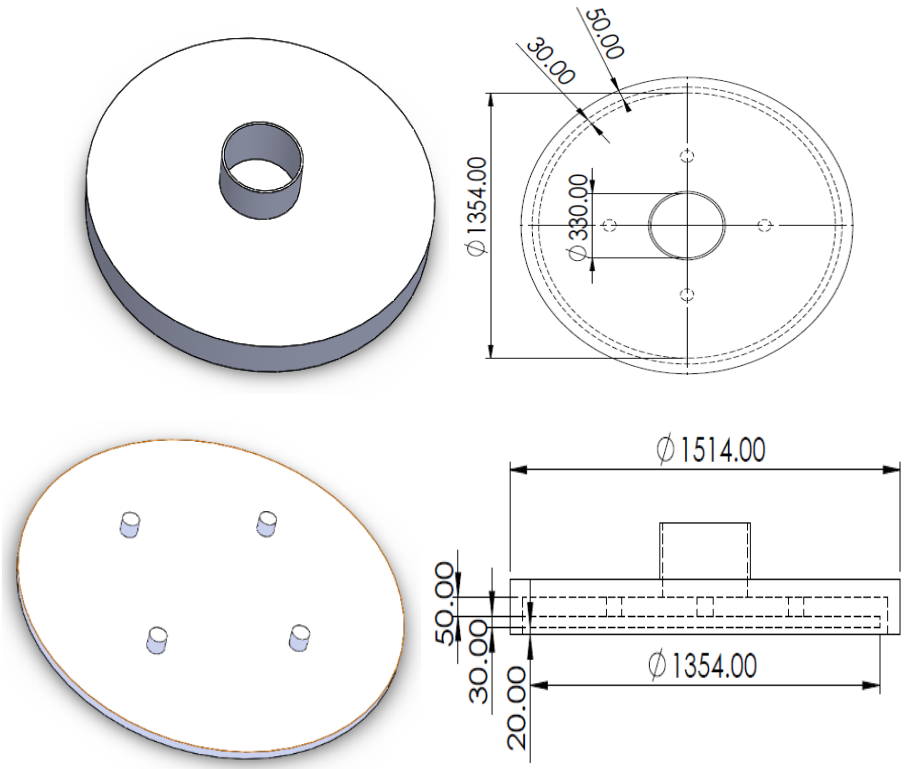

Fig. 2: Circular air cushion model and dimensions

As seen in Fig. 2, we modeled a circular air cushion with its dimensions in SolidWorks. We selected a cushion like Paval et al.'s model [6] for a hovercraft system. The model consists of an inlet channel for the airflow passage. A circular bottom plate is connected to the body via four supporting pins. In this regard, airflow leaves the system through the lateral gap between the plate (pad) and the cushion body. Afterward, we analyzed the CFD of the model using Ansys Fluent software. Note, we also designed different air cushion shapes in SolidWorks, including equilateral triangles, circles, ellipses, rectangles, squares, and four other combined shapes, including circle-rectangles and circle-squares (known as oval shapes), hexagonals, and fillet squares (with two different radii). But after equalizing the cross-sectional area of all shapes and simulating the same for all of them, we found that the cushion with circular geometry creates the most lift force in the same conditions compared to the others. In Fig. 3, we can see the cushion meshing and governing boundary conditions for simulating the system as follows:

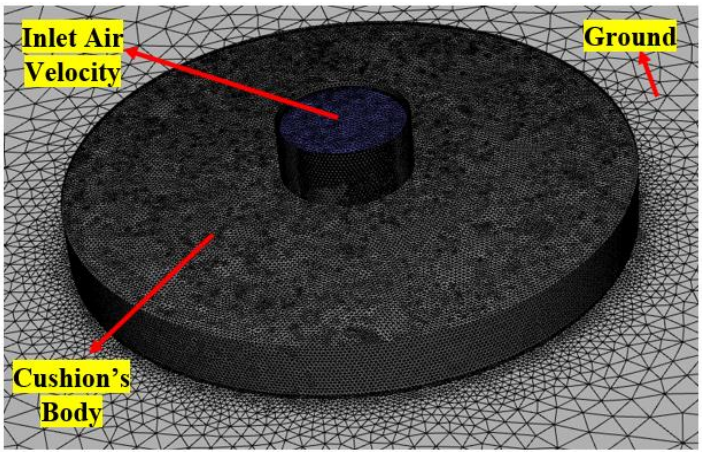

Fig. 3: 3D Meshing of the cushion and governing boundary conditions

After performing several simulations, finally, we obtained a new approximate mathematical formula for calculating the cushion lift force in terms of some parameters containing the inlet airflow velocity, air gap, lateral gap, and Scaling Factor (SF) as follows:

$$F_C(z, y, v', SF) = \delta z^{-2.05} e^{-0.0045y} (v')^{1.985} (SF)^4 \quad (7)$$

where z is the air gap (mm) (between the cushion and ground), y is the lateral gap (mm) (between the pad and cushion body), v' is the air inlet velocity (m/s), SF is the scaling factor, and δ is the geometric shape constant coefficient. For the circular cushion, we have $y = 30\ mm$, $\delta = 739$, $SF = 1$, and $v' = 8.25\ m/s$.

$$F_C(z) = \beta z^{-2.05} \quad (8)$$

Eq. 8 shows the cushion lift force became the only function of the vertical air gap z with $\beta = 42577$. According to the designed system, we evaluated the overall weight of the pod as approximately 26 Tons ($26000\ Kg$). According to Elon Musk's report[1], the outlet pressure of every cushion is approximated with $P = 10\ KPa$. Also, the cross-sectional area of each air cushion is $A_C = 1.44\ m^2$. Thus, the lift force of every cushion will be equal to $F_C = P_C A_C = 14.4\ KN$.

Therefore, we calculated the minimum number of air cushions needed to overcome the overall weight as $N_C = 18$. where N_C is the minimum number of air cushions. For more reassurance, we provided 20 (or 10 pairs) air cushions for the pod suspension.

2.3. Model Verification

The 5-DOF natural frequencies of the system are calculated using the eigenvalues problem method in Eq. 8. Then, the obtained frequencies are compared with the results of vibration simulation of the system in ADAMS software to ensure the correctness of the 5-DOF dynamic equations. In this regard, the same 5-DOF pod with its air cushions and magnets is designed in the vertical and lateral directions in the ADAMS environment as follows:

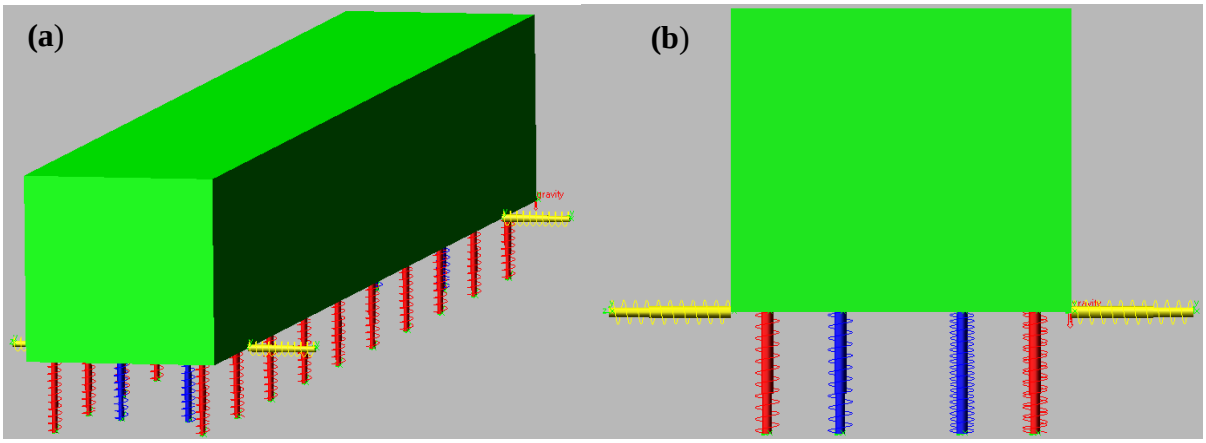

Fig. 4: Simulation of 5-DOF pod model in ADAMS from (a) isometric, (b) front views

According to Fig. 4, the same pod with its suspension systems by modeling air cushions and magnets with linear springs and dampers (the air cushions in red, vertical magnets in blue and lateral ones in yellow color). Also, we defined all dimensions and technical specifications of the previous pod for this simulation model. In addition, we considered all design parameters in the simulated model containing the pod dimensions, total pod mass, the center of mass position $(2.68, 0, -0.56)$, mass moments of inertia of rolling, pitching, and yawing (I_{xx}, I_{yy}, I_{zz}), the location of air cushions and magnets, and the linear stiffness of each of them.

In Table. 1, the system simulation results in the ADAMS software and the obtained analytical eigenvalues (natural frequencies) are compared with each other as follows:

Table. 1: Comparing the eigenvalues of analytical solution with numerical ADAMS

Vibration Mode	Eigenvalue		Eigenvector (Mode Shape)
	ADAMS	Analytical	
1	$\pm 19.123i$	$\pm 19.235i$	$0, -0.9985, 0, 0.03, -0.045$
2	$-0.163 \pm 24.57i$	$-0.169 \pm 24.4i$	$0, 0, 0, 1, 0$
3	$\pm 74.39i$	$\pm 74.75i$	$0, 0.2134, 0, 0.004, -0.977$
4	$-2.561 \pm 95.239i$	$-2.561 \pm 95.239i$	$-0.9927, 0, 0.121, 0, 0$
5	$-6.908 \pm 156.27i$	$-6.908 \pm 156.26i$	$-0.9585, 0, -0.285, 0, 0$

According to Table. 1, we compared the calculated eigenvalues (natural frequencies) from the analytical method with numerical simulation in ADAMS. In Table. 1, it is clear that the results of the eigenvalues obtained from the two methods are very close to each other for the damped system case with $C_a = 10\ \frac{KN.sec}{m}$.

We also obtained the eigenvector in the undamped case to show the pod mode shapes in each vibration mode. Thus, in each vibration mode, any variable that has a higher numerical value (up to the value of 1) will be more excited in that mode. The positive sign means that the movement of the degree of freedom variable is in the same direction as the conventional positive direction defined in the system, and the negative sign shows that the movement of the variable is in the opposite direction and the zero value shows that the variable is not excited in that vibration mode.

3. System Modeling with Compressor Unbalanced Excitation Force

First, we assume that an unbalance driving force due to the rotation of the compressor was created at the end of one of its blades, as modeled in Fig.1:

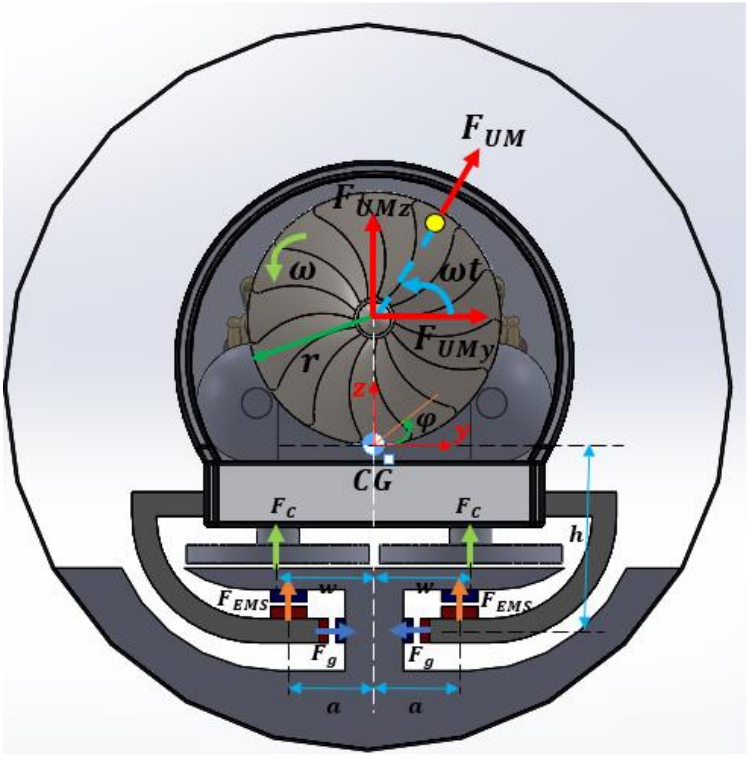

Fig. 5: The compressor's unbalanced force in the proposed pod model

As seen in Fig. 5, the unbalanced driving force with the symbol F_{UM}, resulting in the unbalanced mass m_U, is located at the distance of r from the center of the compressor. Assuming motor-compressor rotation with ω, at any moment of time t, the angular position of the force relative to the center of the compressor spin will be ωt. However, since the force direction always intersects the center of the compressor, transferring it to the center causes its torques to cancel each other. Therefore, we only placed the lateral and vertical forces in the center of the compressor without the torque coupling effect. Considering that, the compressor center is accurately in line with the geometric center of the pod. These forces are also applied in line with the geometric center in front of the pod.

The amount of vertical force will be equal to $F_{UMz} = F_{UM} \sin \omega t$; the amount of lateral force is equal to $F_{UMy} = F_{UM} \cos \omega t$, where $F_{UM} = m_U r \omega^2$. m_U is the unbalanced mass of the blade, and ω is the rotational speed of the compressor in revolution-per-minute or RPM. In this model, the suspension magnetic current is assumed to be stabled and constant with the value of I_0. Therefore, the EMS suspension force formula for both frames will only be a function of the vertical gap z.

Writing the equations in the form $M\ddot{X} + C\dot{X} + KX = F$ again, the external force matrix can be calculated as follows:

$$F = \begin{bmatrix} e\omega^2 \sin(\omega t) \\ e\omega^2 \cos(\omega t) \\ e(\frac{L}{2} - X_{CG})\omega^2 \, sin(\omega t) \\ 0 \\ e(\frac{L}{2} - X_{CG})\omega^2 \cos(\omega t) \end{bmatrix} \quad (9)$$

In Eq. 9, we define $e = m_U r$ as the unbalancing parameter, and X_{CG} is the longitudinal distance between the center of mass and the geometric center. Other matrix coefficients are the same as in Eq. 6.

4. Analytical Determination of System Responses

After determining the coefficient matrix of the equations in the form of $M\ddot{X} + C\dot{X} + KX = F$, in this section, using the Impedance Matrix method, we determine the system's response and natural frequencies through an analytical solution. In this way, assuming the responses initial selection variables and the external excitation forces, respectively, in the exponential form $X = X_0 e^{i\omega t}$ and $F = F_0 e^{i\omega t}$, where $F_0 = e\omega^2$, we have:

$$Z_{ij} = -M_{ij}\omega^2 + C_{ij} i\omega + K_{ij} \quad (i, j = 1,2, \dots, n) \quad [Z]\vec{X} = \vec{F} \quad (10)$$

In Eq.10, $[Z]$ is the impedance matrix, and Z_{ij} is the ith and jth array of the impedance matrix. This matrix is an index to show the system's resistance level against the excitation of external forces. We can calculate the system's natural frequencies using the determinant of the impedance matrix equal to zero as $|Z| = 0$.

In Eq. 10, we can use the following relation to determine the response of the variables of the system:

$$[Z_{5*5}]\vec{X} = \vec{F} \;\rightarrow\; \vec{X} = [Z_{5*5}]^{-1}\vec{F}$$

$$\vec{X} = \frac{1}{|Z|}[A] \begin{bmatrix} e\omega^2 \sin(\omega t) \\ e\omega^2 \cos(\omega t) \\ e(\frac{L}{2} - X_{CG})\omega^2 \, sin(\omega t) \\ 0 \\ e(\frac{L}{2} - X_{CG})\omega^2 \cos(\omega t) \end{bmatrix} \quad (11)$$

In Eq. 11, $|Z|$ is the determinant of the impedance matrix, and $[A]$ is the impedance adjunct matrix. As seen, the product of the inverse impedance matrix in the matrix of external excitation forces is equal to the variables' response. Paying close attention to Eq. 11, it is clear that when the excitation frequency ω caused by the external unbalanced force becomes equal to the natural frequencies ω_n, the

denominator of Eq. 11 or $|Z|$ will be zero, and thus the matrix of the system variables response or $\vec{X}$ will be infinite. Therefore, the system will become unstable. This state of instability is called the Resonance phenomenon. To better and physically show the instability in this case, in the next section, we will discuss the numerical solution of the system, using MATLAB software.

5. Numerical Solutions and Discussions

In this section, we investigate different issues numerically. First, we physically show the resonance occurrence caused by the unbalanced excitation forces. Then we analyze the effects of air cushions' damping and different values of unbalancing on the system oscillations and responses. Finally, we present the influences of the pod's total mass and stiffness of air cushions on the natural frequencies for the undamped system case.

5.1. Resonance Phenomenon

In this section, we examine the state of resonant instability, which means the equality of the external force's excitation frequency with the natural frequencies in the undamped system in the form of a physical representation using equation simulation and numerical solution using MATLAB software.

We calculated the natural frequencies and reported them in Table. 1. Therefore, the excitation frequency of the system in resonance mode is equal to:

$$\omega = \omega_{n3} = 74.75 * \frac{60}{2\pi} = 713.84\, rpm$$

$$\omega = \omega_{n4} = 95.27 * \frac{60}{2\pi} = 909.79\, rpm \quad (12)$$

$$\omega = \omega_{n5} = 156.41 * \frac{60}{2\pi} = 1493.6\, rpm$$

We did not report the first two frequencies because of their low values. Thus, by numerically solving Eq. 6, using the "ode45" command in MATLAB, the results are reported as follows:

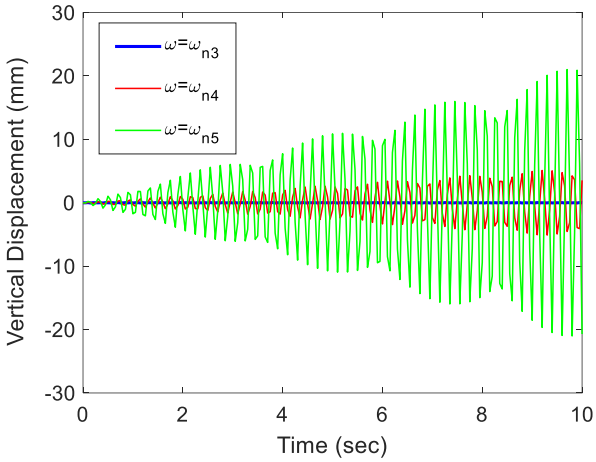

Fig. 6: Vertical displacement instability caused by the resonance phenomenon in the last three vibration modes for the undamped system

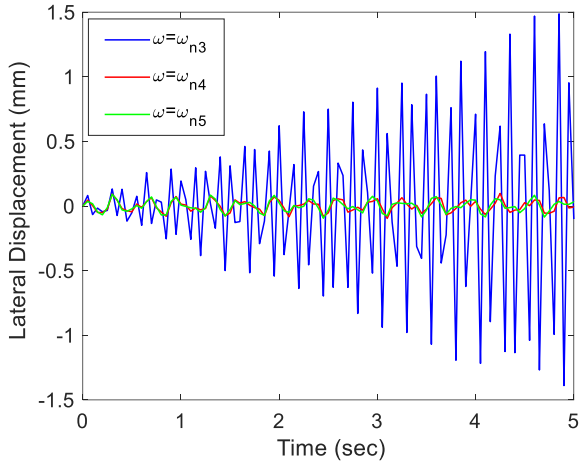

Fig. 7: Lateral displacement instability caused by the resonance phenomenon in the last three vibration modes for the undamped system

Figs. 6-7 show all DOF diagrams according to the simulation time in the resonance state at the last three natural frequencies. We considered the excitation frequency equal to the natural frequencies for the undamped system case. We selected and reported some results showing different behavior over time. In Fig. 7, the lateral displacement (and yawing angle similarly) diverges concerning time, and the system becomes dynamically unstable only for $\omega = \omega_{n3}$. However, Fig. 6 shows that the vertical displacement (and pitching angle similarly) behaves differently. It acts like the "Beating" phenomenon. The oscillations amplitude of the vertical displacement (and pitching angle) more rapidly increases when $\omega = \omega_{n5}$ compared to $\omega = \omega_{n4}$. The beating phenomenon occurs when

the excitation frequency becomes very close (but not equal) to the system's natural frequencies. However, at the beating state, the amplitude of the fluctuations doesn't increase in the subsequently repeated oscillations. But the rolling angle is not changed in the resonance state. Because in this case, according to Eq. 11, there is no external force in the rolling moment equation. Thus, it doesn't affect the rolling angle.

However, we can suggest two practical solutions to deal with and avoid facing this problem. The first and obvious solution is to adjust the compressor engine speed as far as possible from the system's natural frequencies. The second one is to use dampers in the system with sufficient damping, which means that even if the excitation force frequency is equal to the system's natural frequencies, there would be no resonance and divergence of the oscillation range.

Clarifying the issue, we have done another simulation with the damping coefficient of the cushions with three different values as $C_a = 5, 7,$ and $10\ \frac{KN.sec}{m}$ for the last mode resonance as $\omega = \omega_{n5} = 1493.6\ rpm$. We presented the obtained results as follows:

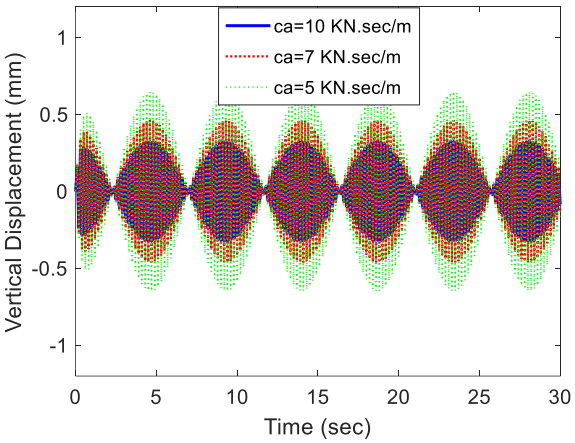

Fig. 8: The pod vertical displacement during the last mode resonance with different air cushions' damping coefficient

As seen in Fig. 8, in the case of the air cushion damping existence, the amplitude of vertical displacement fluctuations (and similarly pitching angle) is not diverged concerning time, even though the force excitation frequency (ω) is equal to the last natural frequency (ω_{n5}). it vibrates at uniform repeating oscillations with a constant period of about 5 seconds with the same amplitude, similar to the beating phenomenon. According to Fig. 8, also it is clear that the amplitude of the oscillations decreases by increasing the air cushions' damping coefficient or C_a.

5.2. Unbalancing Parameter Influence

We simulated other cases with three different values unbalancing parameter (e). Assuming the initial unbalancing parameter as $e_0 = 1.05$, and air cushions damping and the force excitation frequency respectively as $C_a = 10\ \frac{KN.sec}{m}$ and $\omega = 2000\ rpm$, we obtained the following results:

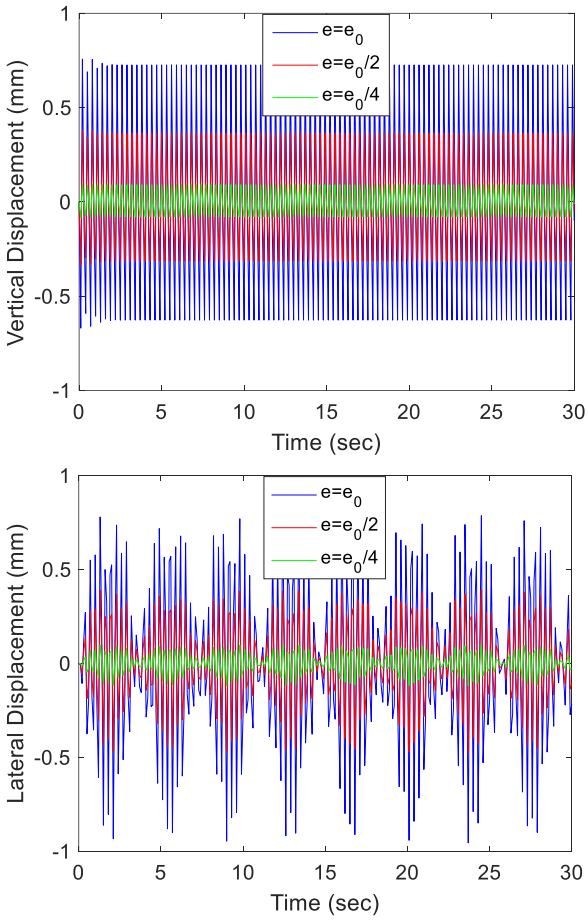

Fig. 9: Vertical and lateral displacement with different values of the unbalancing parameter

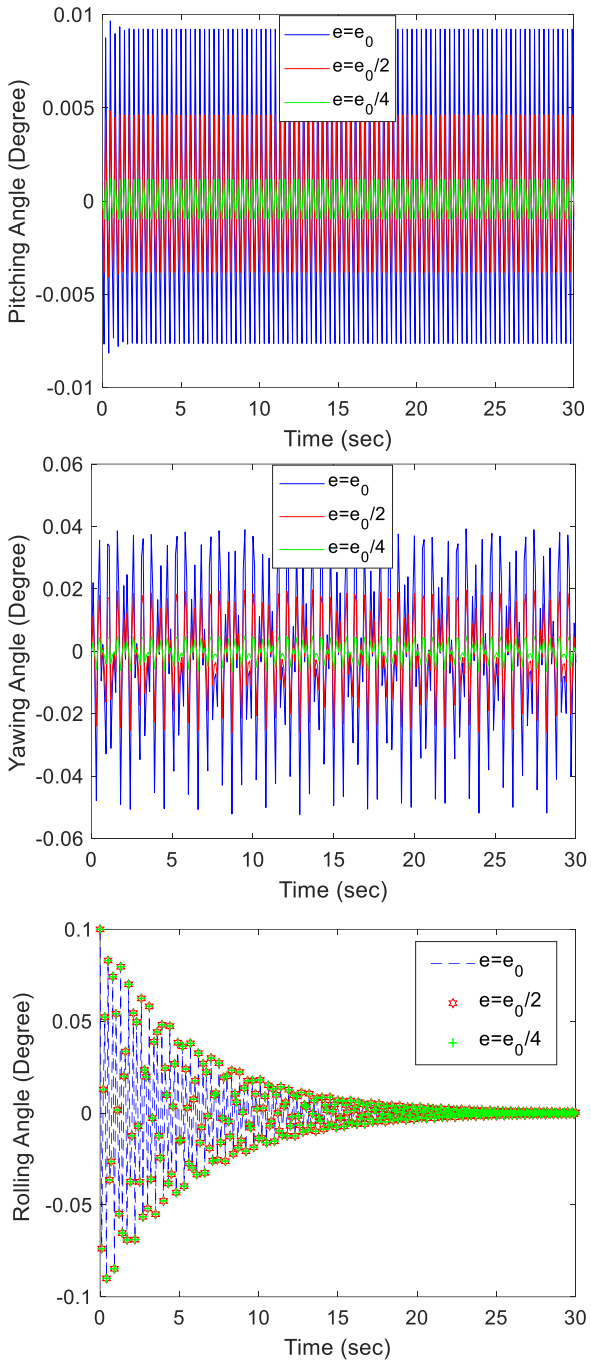

Fig. 10: Body pitching, yawing, and rolling angles with different values of the unbalancing parameter

As seen in Fig. 9 and Fig. 10, the diagram of the vertical and lateral displacements and body pitching, rolling, and yawing angles with various fluctuations repeating in different unbalancing parameter (e) values. According to the diagrams, the oscillations decrease by decreasing the e for every variable except for the rolling angle. Because as mentioned earlier, the external force does not exist in the rolling moment equation. But the rolling angle converged to a stable state over time due to the damping effect of the air cushions.

5.3. Effect of Design Parameters on Natural Frequencies

In this section, we investigated the effect of changing two design parameters on the system's last three natural frequencies. These parameters are the pod's total mass and the air cushions' stiffness. The total mass can be changed by changing the number of passengers, adding or removing cargo, and even changing the choice of materials used in different components. On the other hand, changing the air pressure inside each cushion leads to a change in its equivalent stiffness value. Therefore, we analyzed the variations of these two effective parameters on the natural frequency behavior for the undamped system case as follows:

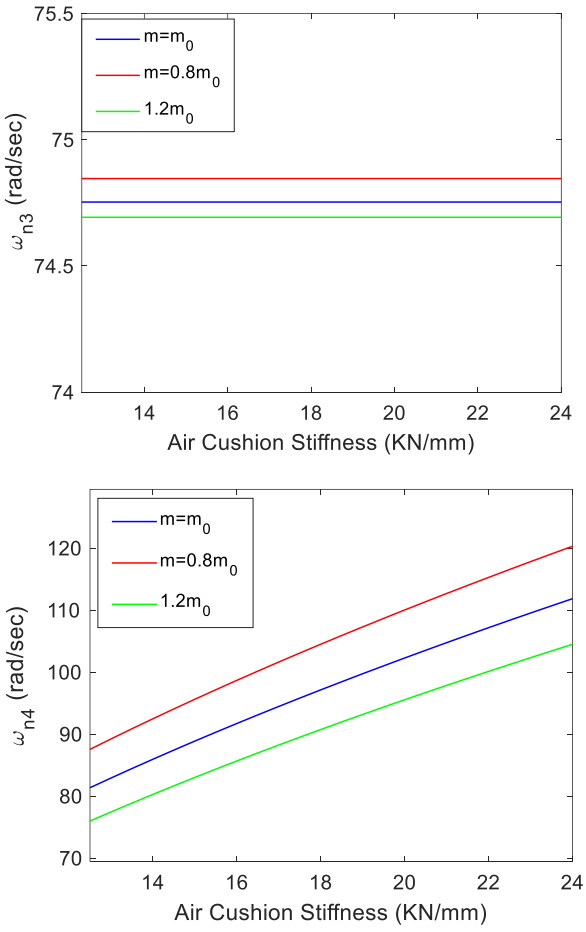

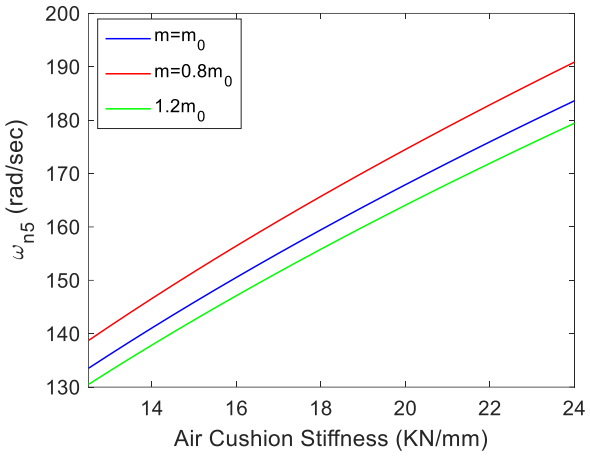

Fig. 11: Air cushion stiffness with different total mass values versus the last three natural frequencies for the undamped system

According to Fig. 11, the last three natural frequencies increased by increasing the total mass, and it decreased by increasing every air cushion stiffness except for the third natural frequency or ω_{n3} for the undamped system. Because the ω_{n3} affects the lateral motion and much more intensively yawing angle (mode shapes of Table.1) and thus, it is related to the lateral movement of the pod. Therefore, the vertical stiffness of air cushions didn't change the ω_{n3}.

6. Conclusions

In this article, we first presented a 5-DOF model for a pod with the conceptually designed model. The proposed pod was equipped with both air cushions and EMS magnets simultaneously. We simulated the system in ADAMS software to verify the proposed model by comparing the obtained natural frequencies of the numerical and analytical methods. Then, we investigated the unbalanced force's influence on the vibration and instability of the pod using analytical and numerical methods. Results showed that the unbalanced force caused creating the resonance phenomenon when its excitation frequency becomes equal to the pod's natural frequencies in the undamped case except for the rolling angle. Also, the system oscillations increase by increasing the unbalancing parameter. The presence of dampers such as air cushions in the system can help to reduce the fluctuations' amplitude and deal with harmful effects of the external disturbing excitation forces and make the pod stable even in the resonance state. Finally, we investigated the effects of varying the pod total mass and stiffness of air cushions on changing the last three natural frequencies. Results illustrated that natural frequencies increased by increasing the total mass and decreasing every air cushion stiffness except for the third natural frequency for the undamped system case.

References

[1] E. Musk, "Hyperloop alpha," *SpaceX: Hawthorne, CA, USA*, 2013.

[2] H.-W. Lee, K.-C. Kim, and J. Lee, "Review of maglev train technologies," *IEEE transactions on magnetics*, vol. 42, no. 7, pp. 1917-1925, 2006.

[3] R. Post and D. Ryutov, "The Inductrack concept: A new approach to magnetic levitation," 1996.

[4] R. Pradhan and A. Katyayan, "Vehicle Dynamics of Permanent-Magnet Levitation Based Hyperloop Capsules," in *ASME 2018 Dynamic Systems and Control Conference*, 2018: American Society of Mechanical Engineers, pp. V002T22A004-V002T22A004.

[5] P. Madhan, S. Gaikwad, and B. Panigrahi, "Design and optimization of nine degrees of freedom suspension model for hyperloop pods," *Proceedings of the Institution of Mechanical Engineers, Part F: Journal of Rail and Rapid Transit*, 2022, doi: 10.1177/09544097221112580.

[6] M. Pavăl, A. Popescu, T. Popescu, D. Zahariea, and D. Husaru, "Numerical study on the movement of air inside the inner cavity of a hovercraft model," in *IOP Conference Series: Materials Science and Engineering*, 2018, vol. 444, no. 8: IOP Publishing, p. 082005.

[7] M. Pavăl, A. Popescu, and D. Zahariea, "Numerical analysis of the influence of the lower hull angle of a round skirtless air cushion vehicle," in *IOP Conference Series: Materials Science and Engineering*, 2019, vol. 595, no. 1: IOP Publishing, p. 012049.

[8] M. Pavăl, A. Popescu, and D. Zahariea, "CFD analysis of a round shaped air cushion vehicle with flexible skirt segments at 90° and different air clearance height," in *IOP Conference Series: Materials Science and Engineering*, 2020, vol. 997, no. 1: IOP Publishing, p. 012151.

[9] M. Pavăl, A. Popescu, and D. Zahariea, "CFD analysis of a round shaped air cushion vehicle with inclined skirt segments," in *IOP Conference Series: Materials Science and Engineering*, 2020, vol. 997, no. 1: IOP Publishing, p. 012152.

[10] K. Wang, W. Ma, S. Luo, R. Zou, and X. Liang, "Coupling vibration analysis of full-vehicle vehicle-guideway for maglev train," *Australian Journal of Mechanical Engineering*, vol. 16, no. 2, pp. 109-117, 2018,doi: 10.1080/14484846.2018.1486794.

[11] B. Wang, Y. Zhang, C. Xia, Y. Li, and J. Gong, "Dynamic analysis of high-speed maglev train–bridge system with fuzzy proportional–integral–derivative control," *Journal of Low Frequency Noise, Vibration and Active Control*, vol. 41, no. 1, pp. 374-386, 2022.

[12] F. Seve, A. Berlioz, R. Dufour, M. Charreyron, F. Peyaud, and L. Audouy, "Balancing of a variable speed rotary compressor: experimental and numerical investigations," 2000.

[13] F. Sève, M. A. Andrianoely, A. Berlioz, R. Dufour, and M. Charreyron, "Balancing of machinery with a flexible variable-speed rotor," *Journal of Sound and Vibration*, vol. 264, no. 2, pp. 287-302, 2003, doi: 10.1016/s0022-460x(02)01173-2.

[14] F. Seve, A. Berlioz, R. Dufour, M. Charreyron, F. Peyaud, and L. Audouy, "On the unbalance response of a rotary compressor," 2000.

[15] G. Ferraris, M.-A. Andrianoely, A. Berlioz, and R. Dufour, "Influence of cylinder pressure on the balancing of a rotary compressor," *Journal of sound and vibration*, vol. 292, no. 3-5, pp. 899-910, 2006.

[16] Q. Wang, J. Zeng, L. Wei, and B. Zhu, "Carbody vibrations of high-speed train caused by dynamic unbalance of underframe suspended equipment," *Advances in Mechanical Engineering*, vol. 10, no. 12, 2018, doi: 10.1177/1687814018818969.

[17] S. A. Jitendrakumar and U. A. Patel, "DESIGN AND IMPLEMENTATION OF PASSIVE LINEAR DYNAMIC VIBRATION ABSORBER FOR VIBRATION CONTROL OF ROTATING MASS UNBALANCE SYSTEM," 2022.

[18] H. Zhang, J. Wu, F. Xie, A. Chen, and Y. Li, "Dynamic behaviors of the crankshafts in single-cylinder and twin-cylinder rotary compressors," *International Journal of Refrigeration*, vol. 47, pp. 36-45, 2014, doi: 10.1016/j.ijrefrig.2014.07.014.

[19] D. S. Aziaka, E. O. Osigwe, and B. T. Lebele-Alawa, "Structural and Conceptual Design Analysis of an Axial Compressor for a 100 MW Industrial Gas Turbine (IND100)," *World Journal of Mechanics*, vol. 04, no. 11, pp. 332-347, 2014, doi: 10.4236/wjm.2014.411033.

[20] D.-J. Min, J.-S. Lee, and M.-Y. Kim, "Dynamic interaction analysis of actively controlled maglev vehicles and guideway girders

considering nonlinear electromagnetic forces," *Coupled systems mechanics*, vol. 1, no. 1, pp. 39-57, 2012.

Appendix

Appendix 1: Proposed pod technical specifications

Parameter	Value	Unit
Pod Overall Length	23	m
Pod Effective Length (L)	19	m
Longitudinal Distance Between Front Magnets and CG (L_f)	4.82	m
Longitudinal Distance Between Rear Magnets and CG (L_r)	10.18	m
Pod Width	2.8	m
Pod Height	2.5	m
Pod Chassis Height	0.3	m
Tube Diameter	6	m
Position of the Pod Center of Gravity (CG) (Relative to the Geometric Center Coordinate)	$x = 2.68\,, y = 0\,, z = -0.56$	m
Mass Moment of Inertia of the Pod Components About CG	$I_{xx} = 713735\,, I_{yy} = 717705\,,$ $I_{zz} = 125420$	$kg.m^2$
Pod Total Mass (m)	25923	kg
Number of Air Cushions	20	$---$
Number of EMS Frames	4	$---$
Each EMS Frame Length	4	m
Lateral Distance Between EMS Magnets ($2a$)	1	m
Linearized Stiffness of Each Frame Vertical Magnets (K_{zj})	1.5395	KN/mm
Linearized Stiffness of Each Frame Lateral Magnets (K_{yj})	2.737	KN/mm
Linearized Stiffness of Each Air Cushion (K_a)	17.3	KN/mm
Lateral Distance Between Air Cushions ($2W$)	2.2	m
Longitudinal Distance Between Air Cushions	2	m
Vertical Distance Between Lateral Magnets and CG (h)	0.96	m
Cross-sectional Area of Each Cushion (A_C)	1.44	m^2
Each Cushion Pressure	10	KPa
Main Compressor Turbine Diameter	2.1	m
Material of Compressor Components	Stainless Steel	$---$
Passenger Capacity	30	$People$
Average Weight of Every Passenger	75	kg